The Effect of Crystallization Conditions on the Properties of Polyoxymethylene

C. J. G. PLUMMER,[1,*] P. MENU,[1] N. CUDRÉ-MAUROUX,[2] and H.-H. KAUSCH[1]

[1]Laboratoire de Polymères, Ecole Polytechnique Fédérale de Lausanne, CH-1015 Lausanne, Switzerland; [2]DuPont de Nemours Int., Le Grand Saconnex, CH-1218 Geneva, Switzerland

SYNOPSIS

Measurements using compact tension specimens machined from compression and injection-molded plaques of polyoxymethylene show a systematic decrease in the plane-strain critical stress intensity K_{IC} for crack initiation with crystallization temperature and with molecular weight, but little change in the yield stress in plane strain compression tests. The variation in K_{IC} with crystallization temperature has been accounted for in terms of the effective entanglement density in the damage zone ahead of the crack tip. The entanglement density is argued to decrease with increasing temperature owing to partial disentanglement of the polymer chains during lamellar folding. © 1995 John Wiley & Sons, Inc.

INTRODUCTION

The object of the present work was to account for the fracture behavior of polyoxymethylene (POM) in terms of its molecular structure. Although POM is semicrystalline, and well above its glass transition at room temperature, parallels may be drawn between its deformation behavior and that of amorphous glassy thermoplastics. Yielding in bulk POM is accompanied by extensive cavitation, giving rise to localized cracklike voided damage zones.[1-3,†] These structures are qualitatively similar to crazes in amorphous polymers in the glassy state.[4] In each case, the damage zone is characterized by a network of highly extended fibrils running perpendicular to its length and linked at irregular intervals by so-called cross-tie fibrils.[4,5]

In view of these similarities, it is reasonable to assume that similar mechanisms govern stable crack propagation and initiation in POM and crack propagation in a glassy polymer via breakdown of fibrils in the craze running ahead of a crack tip. In this latter case, according to Brown,[6] under small-scale yielding conditions (SSY), we have

$$K_{IC} = \left[\frac{2\pi(1-\mu^2)ED_0}{S_c}\right]^{1/2} \alpha^{1/4} \times (1-1/\lambda)^{1/2} f_s \nu_e d_e/2 \quad (1)$$

where D_0 is the fibril spacing; α reflects the elastic anisotropy of the craze; λ is the draw ratio of the craze fibrils; E, the bulk tensile modulus modulus; μ, Poisson's ratio; and S_c, the craze widening stress. The term $f_s\nu_e d_e/2$ arises from the use of the entanglement network model for the effect of topological constraint on chain motion in the glassy state. The number of entangled strands crossing the unit surface area in the undrawn polymer is approximately $\nu_e d_e/2$, where ν_e is the entanglement density, and d_e, the rms spatial separation of topologically linked entanglement points.[4] f_s is the force required to break or disentangle one such strand; hence, $f_s\nu_e d_e/2$ is approximately the breaking stress of one fibril. The local critical stress intensity at the crack tip k_c is then equated to $(\pi D_0)^{1/2} f_s \nu_e d_e/2$ and eq. (1) is obtained by relating k_c to the global critical stress intensity K_{IC}. This approach has been shown to be consistent with data for crack propagation in PMMA, given reasonable estimates of the various quantities involved,[6] and its essential correctness has been verified in detail by other workers.[7]

* To whom correspondence should be addressed.

† For POM, the characteristic ratio $C_\infty \sim 10$, so that $\lambda \sim 0.8(n/C_\infty)^{1/2} \sim 4$, where $n = 2M_e/M_0 = 3100/15$ is the number of main chain bonds per entanglement (M_0 is the monomer molecular weight).

Journal of Applied Polymer Science, Vol. 55, 489-500 (1995)
 CCC 0021-8995/95/030489-12

In POM, the assumption of a strip yield model is no longer justified, deformation ahead of the crack tip consisting of a dense, approximately cylindrical bundle of crazes. As discussed in more detail in Ref. 8, compact tension tests give K_{IC} values for crack initiation in POM, rather than propagation, and the problem of relating K_{IC} to k_c is more akin to that of crack-tip shielding by microcracking (as in certain ceramics). Nevertheless, one expects the K_{IC} to remain proportional to k_c under such conditions (the constant of proportionality being a function of the ratios of the elastic constants in the crazed and uncrazed material) and, hence, K_{IC} should scale as $D_0^{1/2} f_s \nu_e d_e$ as in eq. (1), where ν_e is the effective entanglement density. In this approach, the surface density $\nu_e d_e$ takes the place of the tie molecule density often invoked in discussions of the fracture toughness of semicrystalline materials. One of our main assumptions is therefore that in addition to true tie molecules topological constraints trapped in the interlamellar layers on solidification will play an important role in the ultimate properties of the cohesive zone.

For crystallization at high supercoolings, the entanglement network parameters in POM are expected to remain similar to those in the melt[3]; hence, injection-molded POM samples, which are generally subject to relatively high cooling rates, provide a convenient reference state. During crystallization at higher temperatures, however, where crystallization rates are lower, $\nu_e d_e$ is likely to decrease owing to entanglement loss. The chain mobility is higher and there is more time for disentanglement. We estimate the extent of entanglement loss in the fourth section, Predicting Entanglement Loss During Crystallization, by considering changes in the lamellar thickness with crystallization temperature, the overall spherulitic growth rate, and the extent of chain relaxation in the crystallizing melt. Results from microstructural characterization of the samples required for the fourth section are given in the section Physical Characterization. Discussion of K_{IC} data for compact tension specimens of POM compression-molded at various temperatures is deferred until the section Mechanical Behavior, however, where they are compared with the predicted evolution in K_{IC} based on the results of the fourth section.

EXPERIMENTAL

Three grades of POM with number-average molecular weights, M_n, of 66×10^3, 41×10^3, and 35×10^3 were available as pellets (containing stabilizers) and as injection-molded plaques supplied by DuPont de Nemours. Compression molding of the pellets was carried out in-house using a Bucher-Guyer LS 35 press at 145, 147, 150, and 160°C after prior melting at 200°C, with an applied pressure of approximately 5×10^5 Nm^{-2}, giving circular plaques of diameter 93 mm and thickness of approximately 8 mm. Compact tension (CT) specimens were machined from the plaques as illustrated in Figure 1(a) and a natural crack introduced at the notch tip using a fresh razor blade. K_{IC} was then measured on a Zwick 1484 tensile test machine at a crosshead speed of 1 mm/min, following the protocol established in Ref. 9. To estimate the yield stress, plane strain compression tests[10] were carried out on 3×15 mm cross-section strips of approximately 10 cm in length, using the test geometry illustrated in Figure 1(b).

Thermal characterization was carried out using the Perkin-Elmer DSC 7. The DSC was calibrated using indium and zinc, using extrapolation to the zero ramp rate of melting point data at a fixed sample weight and various ramp rates to set the temperature scale. All subsequent measurements of the

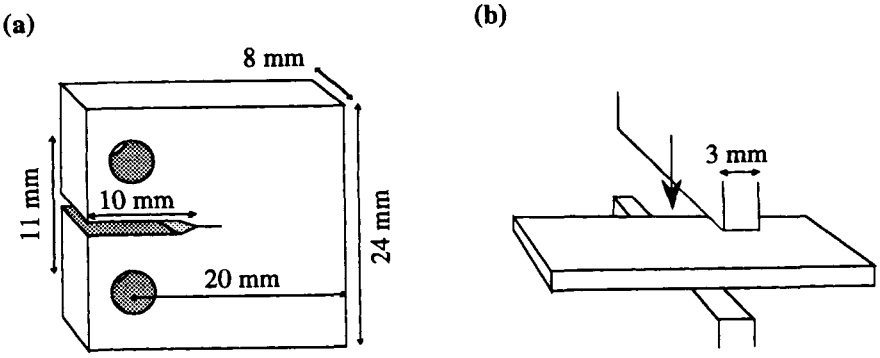

Figure 1 (a) The geometry of the CT specimens; (b) the plane-strain compression test.

melting point (T_m) were carried out for a sample weight of 3 mg and similarly extrapolated to the zero ramp rate. Isothermal crystallization was carried out in the DSC at various crystallization temperatures (T_c) in order to determine $T_m(T_c)$ and appropriate crystallization times for compression molding (crystallization was assumed complete when there was no further detectable change in enthalpy, at which point the samples were cooled to 30°C).

Measurements of the radial spherulite growth rate (G) were carried out under nitrogen using melted films compressed between two glass coverslips, placed on a Linkam hot stage. Observations were made in transmitted light using crossed polarizers and growth rates measured from video recordings. To measure growths at high undercoolings, powder samples were sprinkled onto the coverslips to give a dispersion of fine droplets, nucleation being delayed in certain droplets.

PHYSICAL CHARACTERIZATION

DSC Measurements

Figure 2 shows $T_m(T_c)$, $\Delta H(T_c)$, and the half-times for crystallization for each of the grades taken from the isothermal measurements (below 150°C recrystallization during scanning invalidates T_m and ΔH measurements in POM).

The melting-point depression for a mean lamellar thickness l is estimated from

$$T_m = T_{m0}\left(1 - \frac{2\sigma_e}{\Delta h_0 l}\right) \qquad (2)$$

where T_{m0} is the equilibrium melting temperature, estimated from $T_m(T_c)$ to be 200°C, in agreement with values currently found in the literature obtained by a variety of techniques,[11-15] σ_e is the fold surface energy, and Δh_0, $\sim 380 \times 10^6$ Jm^{-3}, is the heat of fusion per unit volume of the crystalline phase.[16] Assuming lamellar thickening by a factor γ behind the advancing lamellar front,[17] then

$$l = \gamma l^* \sim \gamma \frac{2\sigma_e T_{m0}}{\Delta h_0 \Delta T} \qquad (3)$$

where l^* is the initial lamellar thickness as predicted from kinetic theory and $\Delta T = T_{m0} - T_c$.[18] Combining eqs. (2) and (3) allows one to determine γ from $T_m(T_c)$,[19] which gives a constant value of approximately 2 for $T_c > 150$°C. In order for eq. (3) to be useful as an analytical expression for l, it is necessary to estimate σ_e. This was done by fitting eq. (3) with $\gamma = 2$ to data obtained from small-angle X-ray scattering (SAXS) on samples with $M_n = 35 \times 10^3$ (Ref. 20) (similar results were obtained by Salaris et al.,[15] again using X-ray techniques). Good agreement was obtained by taking $\sigma_e = 1.25 \times 10^{-1}$ Jm^{-2}, as shown in Figure 3, along with values for l calculated from eq. (2) using DSC data for T_m. The low-temperature values for l are consistent with direct observations of lamellar thicknesses by TEM in injection moldings.[3]

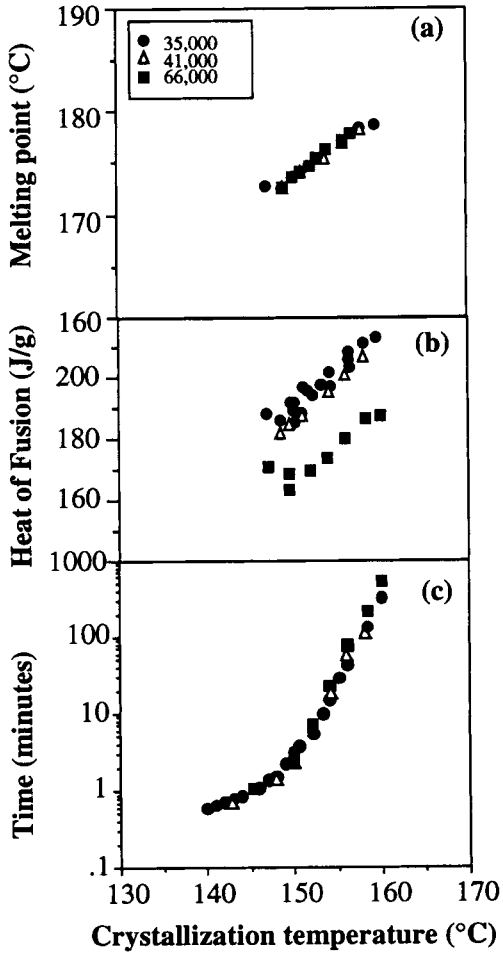

Figure 2 (a) T_m as a function of T_c; (b) ΔH as a function of T_c; (c) crystallization half-times as a function of T_c.

Spherulite Growth Rate Measurements

Growth rate data are given in Figure 4 for POM, $M_n = 66 \times 10^3$ (similar results were obtained for the other molecular weights). In agreement with earlier results,[21] plots of $\log G + Q_d/2.3RT$ against $1/T\Delta T$ were found to be approximately linear, with an ap-

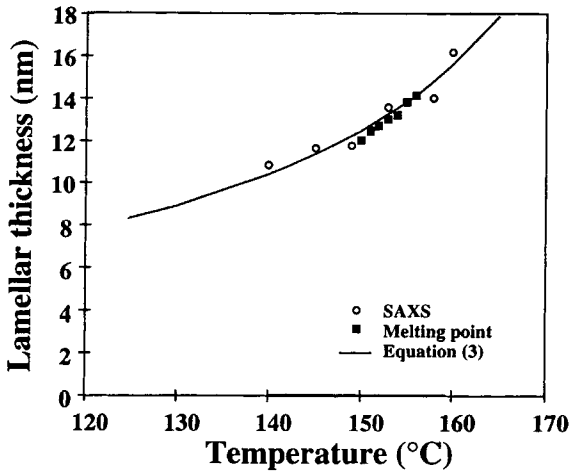

Figure 3 Data for the lamellar thickness for $M_n = 35 \times 10^3$ compared with a fit using eq. (3) and melting point data.

parent change in slope by a factor of 2 at approximately 160°C. (Q_d was taken to be 30,000 $Jmol^{-1}$ [Ref. 21], although assumptions about the temperature dependence of the transport term are not critical and much the same results are obtained using the WLF formulation.)

The equations of the fitted curves, which have been superposed on the data in Figure 4, are

$$\log G_{III} + Q_d/2.3RT = 7.7 - 1.96 \times 10^5/T\Delta T \quad (T < 160°C)$$

and

$$\log G_{II} + Q_d/2.3RT = 2.0 - 0.98 \times 10^5/T\Delta T \quad (T > 160°C) \quad (4)$$

where G_{III} and G_{II} refer to the regime III (secondary nucleation) and regime II (combined secondary nucleation and lateral growth) mechanisms proposed in Refs. 21 and 22 to account for this behavior. Regardless of the validity of this interpretation, eq. (4) provides a convenient analytical form for $G(T)$.

PREDICTING ENTANGLEMENT LOSS DURING CRYSTALLIZATION

Chain Mobility and Crystallization Rates

It was first recognized by Flory and Yoon[23] that if the time scales associated with crystallization are much shorter than those associated with disentanglement, then the chain conformation, and, hence, the topology of the melt state, should survive in the semicrystalline state, consistent with neutron scattering results for crystallization at high supercoolings in polyethylene (PE) and isotactic polystyrene (iPS).[24,25] Under such conditions, the semicrystalline state should therefore show the same degree of entanglement as does the melt. For the purpose of this section, we assume that at high supercoolings lamellar growth occurs by secondary nucleation and that there is negligible lateral growth of a given nucleus subsequent to its formation. This is equivalent to the regime III described by Hofmann,[21] and on the basis of an analysis of the spherulite growth data in Figure 4 in terms of a regime change, the assumption of secondary nucleation controlled growth would appear justified up to the highest crystallization temperatures used for the mechanical tests (160°C).

We know of no evidence that directly contradicts this assumption in the specific case of POM. Nevertheless, it must be qualified in so far as many, if not all, aspects of Hoffman's interpretation are extremely controversial.[26,27] The role of secondary nucleation is perhaps more widely accepted,[28] but the problem is that here we take each nucleus to be as-

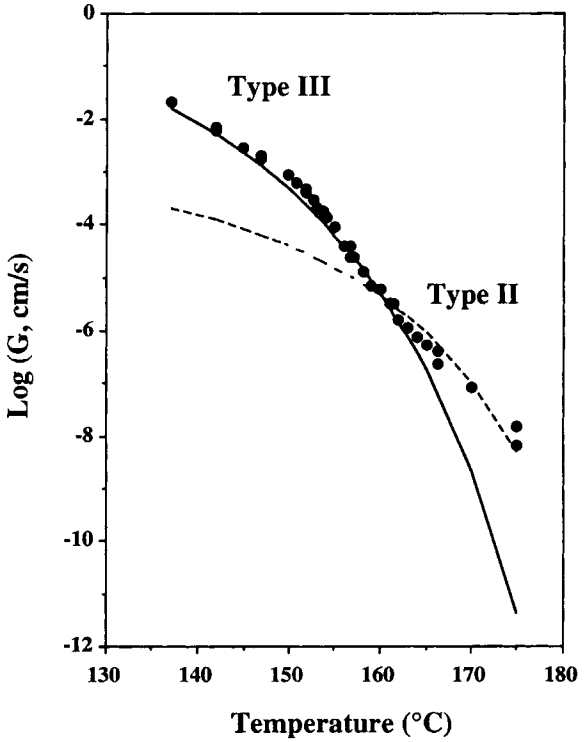

Figure 4 Radial spherulite growth rates for $M_n = 66 \times 10^3$, compared with Hoffman's equations (hatched line, regime II; solid line, regime III).

sociated with three adjacent re-entrant folds, so that the amount of polymer chain needed to accommodate the nucleus depends only on the lamellar thickness. However, whereas lateral growth will tend to increase the number of folds associated with the nucleus, since both the extent of lateral growth and the lamellar thickness may both reasonably be expected to increase with crystallization temperature, the same qualitative trends are expected, whether one includes lateral growth or not. Therefore, in excluding lateral growth, we calculated degrees of entanglement loss that might be considered lower limits within the wider framework of secondary nucleation theory.

To investigate the conditions under which there is no entanglement loss, and the degree of entanglement loss at higher temperatures, we used the model of Klein and Ball,[29] which describes the dynamic response of an entangled chain to lamellar folding in terms of the short-range "reeling-in of slack," and in which steady-state "forced" reptation is a limiting case (we do not, however, require that reptation be the rate-controlling step in lamellar growth in this limit). Following the tube model of DeGennes,[30] Klein and Ball associated C, the stored length/unit length of tube (the "slack"), with a certain density of chain defects within the tube. Regions of the chain already attached to a lamella were treated as perfect defect sinks ($C = 0$), and transient configurational changes were modeled in terms of the diffusion of defects toward such sinks.

Prior to the first secondary nucleation event, $C = C_0$ everywhere along the chain. The first secondary nucleation event is assumed to take place relatively rapidly, since it will require only very local conformational arrangements and, hence, to be equivalent to a rapid "tug" on the chain, reducing C to 0 in the immediate vicinity of the nucleus. In the absence of further nucleation, equilibrium will eventually be reestablished, C will rise to C_0, and the tube will be shortened by an amount corresponding to the length of chain in the nucleus. If x is the distance along the tube over which the perturbation in C has propagated at time t, then in the case of a chain that has nucleated at one of its ends (the most extreme case), then

$$\frac{x}{L} = \frac{\pi(\Delta t)^{1/2}}{L} = \pi\left(\frac{kTt}{LC_0^2 d_e n_0 \xi_0}\right)^{1/2} \sim \pi\left(\frac{kTt}{C_0^2 n_0 \xi_0}\right)^{1/2} \frac{1}{r_0} \quad (5)$$

where L is the tube length; Δ, the defect diffusion constant; C_0, the equilibrium stored length/unit length of tube; d_e, the tube diameter; n, the number of monomers per chain; ξ_0, the monomeric friction coefficient; and r_0, the rms end-to-end distance of the chain.[29]

The time τ_d at which $x/L = 1$ is the time at which steady-state reptation is established. The condition for steady-state reptation is therefore that $\tau_d < \tau_c$, where τ_c is the time between nucleation events on a given chain. This is because secondary nucleation within a given chain will effectively pin the chain in its tube and prevent further reptation, further growth being possible only by depletion of slack within the resulting trapped loops.

To estimate τ_d, we used the method of Van Krevelen[31] to estimate the magnitude of ξ_0 for POM in the relevant temperature range. The temperature dependence of the Newtonian viscosity $\eta_0(T)$ was obtained using the empirical formula

$$\log[\eta_0(T)] = \log[\eta_0(1.2T_g)] + A\left(\frac{T_g}{T} - 1\right) \quad (6)$$

assumed to be valid for $T_g/T < 0.6$, where for POM, $A \sim 7.33$, and $\log[\eta_0(1.2T_g)] \sim 5.65 + 3.4 \log(M/2M_e)$. M_e, the entanglement molecular weight, is taken to be 3100.[16] ξ_0 is then obtained from

$$\xi_0 = \frac{10kT\eta_0(T)J_{e0}(T)}{n_0}\left(\frac{d_e^2}{r_0^4}\right) \quad (7)$$

where $J_{e0}(T)$ is the plateau compliance, given by $J_{e0}(T) = (3/2)M_e/\rho RT$,[31] and using $r_0 \sim 30$ nm for $M = 66 \times 10^3$ and $d_e \sim 6.6$ nm.[3,16] $C_0 \sim \lambda - 1$ is estimated to be 3 for POM, given that $\lambda = 4$.[3]

τ_c is estimated from the time taken for the growth front to incorporate a chain, given by r_0/G divided by N_c, the number of nuclei per chain. This latter quantity is the number of chains per unit volume $L_A\rho_s/M$ divided by the number of nuclei per unit volume, where ρ_s is the density of the solid polymer, and L_A, Avogadro's number. The volume of one nucleus is assumed to be $3b_0a_0l^*$, where b_0 is the fold separation parallel to the growth direction; a_0, the fold separation perpendicular to the growth direction, and l^*, the initial lamellar thickness. The factor of 3 arises since, as will be discussed in the next subsection, we assume each nucleated stem to contain three adjacent reentrant folds. The number of nuclei per chain is then

$$N_c \sim \frac{\chi M}{3L_A\rho_s b_0 a_0 l^*}$$

where χ is the degree of crystallinity, and

$$\tau_c = \frac{3L_A\rho_s b_0 a_0 l^* r_0}{\chi MG} \tag{8}$$

τ_c is compared with the time τ_d at which $x/L = 1$ for different molecular weights in Figure 5, taking $a_0 b_0 \sim 1.715 \times 10^{-19}$ m^2,[21] $\rho_s \sim 1400$ kg^{-3}, and $\chi \sim 0.7$ (the choice of χ is not critical). This suggests that forced reptation may be possible down to about 145°C, i.e., well into the temperature range in which Hofmann suggested regime III growth to occur in POM,[21] and that it is only at temperatures less than 145°C that the first nucleation event in a given chain will not affect the overall chain configuration.

Estimating the Degree of Entanglement Loss

The choice of three for the number of adjacent reentrant stems per nucleus in nucleation controlled growth arises from a statistical requirement for a certain degree of adjacent reentrant chain folding; if there were no adjacent reentry, the density at the interface between the lamellae and the amorphous regions would have to be approximately three times that in the lamellae to accommodate the change from an oriented to a random configuration. Thus, on average, there must be at least three stems associated with each chain emerging from a given lamellar surface, i.e., a degree of adjacent reentry of at least three.[21,32] That the degree of adjacent reentry is limited to three at high supercoolings, where nucleation is believed to occur, has been shown to be consistent with neutron scattering results.[24,25]

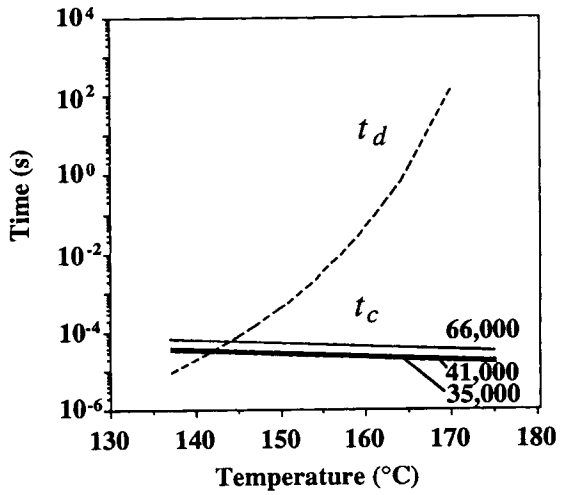

Figure 5 Comparison of the time between nucleation events (hatched curve) in a given chain and the time for the establishment of steady-state reptation in regime III (solid curves).

The extent to which crystallization involves entanglement loss depends on how much the tube length is changed. Given the results of the last subsection, the tube length may be taken to be unchanged for $T_c < 145$°C and so the entanglement density will be that of the melt, as assumed previously [Fig. 6(i)]. Where the chain is able to reptate, however, entanglement may be lost in spite of pinning by secondary nucleation. After the first nucleation event, the tube will shorten by a certain length that will depend on the total length needed to form the nucleus. Whereas the next two nucleation events in the same chain will result in trapped loops, a further length may be lost from the free ends and so forth [Fig. 6(ii)]. After completion of crystallization, the tube length will be shortened by some length ΔL. Since $L = Md_e/M_e$, and assuming d_e to remain unchanged (the chain effectively slips through the entanglement constraints), the effective entanglement molecular weight M_e' for the shortened tube becomes

$$M_e' = \frac{M_e L}{L - \Delta L} = \frac{M_e}{1 - \Delta L M_e/Md_e}$$

or, since ν_e is proportional to $1/M_e$,

$$\nu_e = \nu_{e0}(1 - \Delta L M_e/Md_e) \tag{9}$$

where ν_{e0} is the density in space of the entanglement points in the absence of disentanglement. Values of ΔL have been estimated according to the scheme sketched in Figure 7. A group of three lamellar stems associated with a total molecular weight M_l is taken to shorten the tube by a length $d_e M_l/2M_e$ at either end, unless other nuclei are present between it and one or both of the free ends of the chain. The reason for using l^* here is that it is assumed that the topology of the network is determined by the initial phase of lamellar formation and is relatively little affected by subsequent lamellar thickening, which is assumed to take place by local chain slip and redistribution of slack (through remelting of subsiduary lamellae, e.g.). Note also that for this simple calculation no attempt has been made to take into account lamellar thickness distributions or the effect of the orientation of the lamellae with respect to the tube.

To estimate the changes in ν_e, a given tube is subdivided into N lengths approximately equal to d_e, numbered sequentially from one end. Nucleation is then assumed to occur with equal probability at any

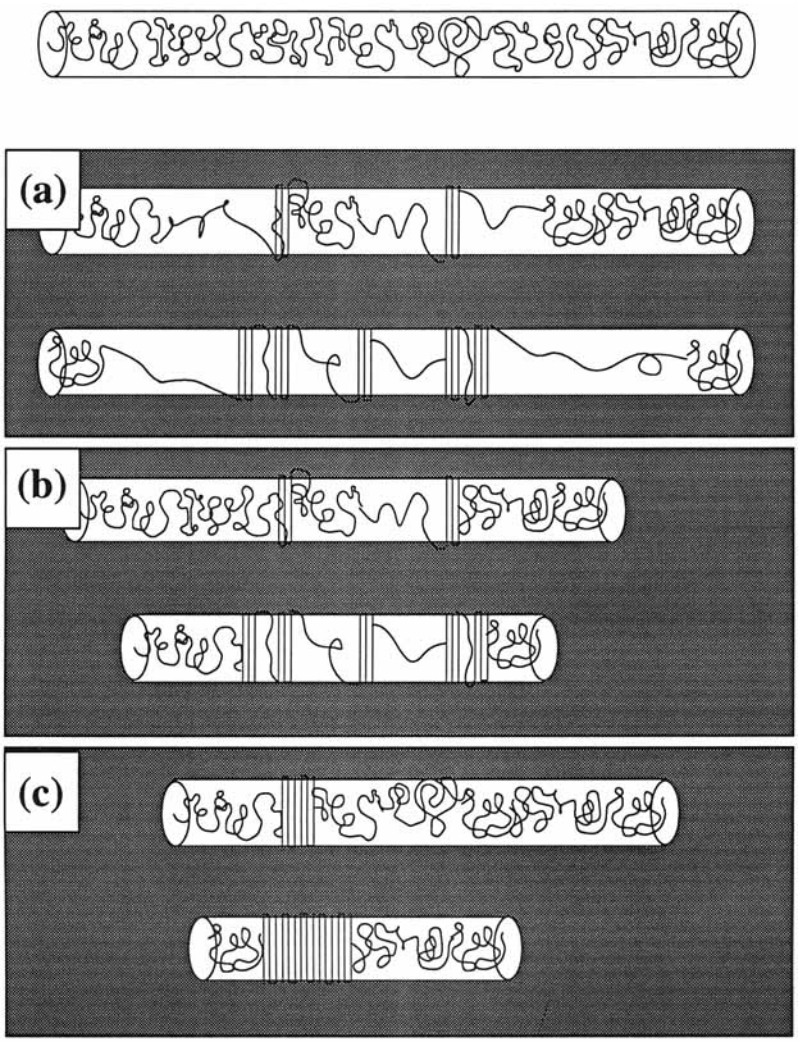

Figure 6 Schematic of transport mechanisms during crystallization using the tube model (in each case, the state of the chain after successive nucleation events is shown; note that in reality the tube will adopt a 3-D Gaussian configuration): (a) Reeling in of slack only; nucleation occurs too rapidly to allow full relaxation of the chain and so the tube length does not change as a result of chain folding. (b) Reptation limited by nucleation; the tube may shorten, but loops of amorphous chain pinned by nuclei do not attain their equilibrium conformation. (iii) Sideways growth of a single nucleus; no temporal or physical constraints on reptation.

of the $1 \cdots N$ sites unless there remains insufficient free length or slack to accommodate three stems. Nuclei are added one after the other to the chain, at randomly selected sites. Sites already occupied by a nucleus, sites beyond the current position of one or other of the chain ends, and sites associated with insufficient free length or slack to form a nucleus are discounted. When no further nucleation is possible, the resulting value of ΔL is used to calculate ν_e according to eq. (9). Results of such simulations are given in Table I for different M and temperatures.

MECHANICAL BEHAVIOR

Entanglements and Tie Molecules

Cohesion in semicrystalline polymers is frequently discussed in terms of tie molecules. Since r_0, in general, exceeds the lamellar period, different parts of a single molecule may be incorporated simultaneously in two or more lamellae, forming a molecular bridge or tie molecule. The resulting tie molecule density in rapidly cooled samples of POM has been estimated from the low-temperature brittle strength

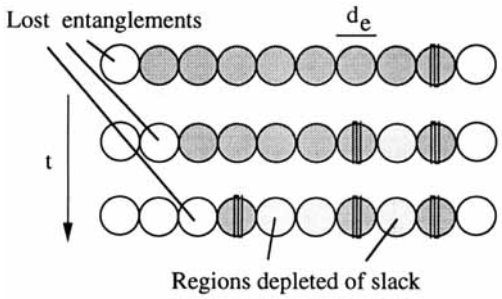

Figure 7 Schematic of the calculation of entanglement loss in regime III; heavily shaded regions contain the equilibrium amount of stored length, lightly shaded regions are depleted of stored length, and unshaded regions are those from which the chain has been drawn out by reptation.

and suggests that approximately 15% of the lamellar stems to be associated with a tie molecule.[33] Given a stem density N_f of approximately 6×10^{18} m^{-2}, there are, therefore, approximately 9×10^{17} tie molecules per unit area of lamella. In the entanglement model, given $\nu_e = 10^3 N_A \rho_a / M_e = 24 \times 10^{25}$ m^{-3} (using $\rho_a = 1250$ kg^{-3} and $M_e = 3100$) and $d_e = 6.6 \times 10^{-9}$, if a correction factor of $(\rho_s/\rho_a)^{2/3}$ is assumed, where $\rho_s = 1400$ kg^{-3} is the density of semicrystalline POM, we estimate $\nu_e d_e \sim 1.7 \times 10^{18}$ m^{-2}. Thus, the number of the entangled strands crossing unit area is given by $\nu_e d_e/2 \sim 8.5 \times 10^{17}$ m^{-2}.

This agreement should be considered in the light of the large approximations involved in the experimental determination of the tie molecule density. However, it does suggest that the observed tie molecule densities are consistent with the entanglement network's having been frozen into the crystalline state of POM. This is readily explicable if one assumes the experimental tie molecule densities to take into account not only true tie molecules, but also trapped loops and other topological constraints. Indeed, for final lamellar thicknesses of the order of 10 nm as estimated from eq. (3) for crystallization at 130°C, very few "true" tie molecules are anticipated. A method for calculating the tie molecule density has been suggested by Gedde and Jansson.[34]

Table I Estimates of ν_e for a Variety of Conditions

T_c	$M = 66 \times 10^3$	$M = 41 \times 10^3$	$M = 35 \times 10^3$
130°C	ν_{e0}	ν_{e0}	ν_{e0}
150°C	$0.81\nu_{e0}$	$0.71\nu_{e0}$	$0.68\nu_{e0}$
160°C	$0.76\nu_{e0}$	$0.64\nu_{e0}$	$0.62\nu_{e0}$

Assuming no lamellar tilting, the proportion of stems associated with a tie molecule is given as

$$\frac{1 - N_A \rho_c l / \chi M N_f}{1 + \rho_c l (1 - \chi)/\chi \rho_a b} \tag{10}$$

where b is the step length, approximately equal to 1 nm for POM. For $l = 10$ nm and $M = 66 \times 10^3$, taking $\chi = 0.6$, eq. (10) gives a value of approximately 5% (similar values were estimated for PE of comparable molecular weight[34]).

Predicting K_{IC}

The effective entanglement density in the damage zone ν_e' is taken to be

$$\nu_e' = \nu_e \left(1 - \frac{M_e}{M_n}\right) \tag{11}$$

assuming regions less than one entanglement length away from the chain ends to be unable to contribute to the network. Where there is disentanglement during crystallization, M_e in eq. (11) should be replaced by $M_e' = M_e \nu_{e0}/\nu_e$ using the values in Table I. The estimated changes in K_{IC} with crystallization temperature arising from changes in ν_e (as given in Table I) are shown in Figure 8, where $K_{IC} = K(\nu_e'/\nu_{e0})$ is given for different crystallization tem-

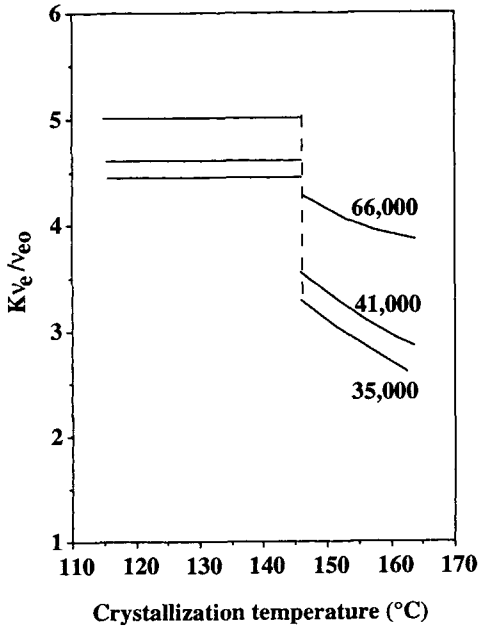

Figure 8 Estimates of K_{IC} from the entanglement density; K is chosen such that $K\nu_e'/\nu_{e0} = 5$ for $M = 66 \times 10^3$ at the lowest crystallization temperature.

peratures (d_e is assumed constant, and for the moment, we assume f_s to be independent of M). The front factor K was chosen to facilitate comparison with the experimental data in the following section and was assumed constant. Although the inclusion of the chain end correction in eq. (11) is difficult to justify in detail, comparison of Figure 8 and Table I indicates that it makes a relatively small difference to the final result.

Comparison with Experimental Values

For the compression moldings molded at 150°C, crystallization times of approximately 1 h were used, which was adequate to ensure full crystallization in the DSC at this temperature. The measured melting point of these plaques was between 172 and 173°C, consistent with that of samples crystallized in the DSC. In the case of the samples molded at 160°C, the crystallization time was limited to 6 h owing to problems with degradation. Although this was adequate to ensure full crystallization for $M_n = 35 \times 10^3$ in the DSC, this was not the case for the higher molecular weights. Indeed, whereas the $M_n = 35 \times 10^3$ had a melting point of approximately 178°C,

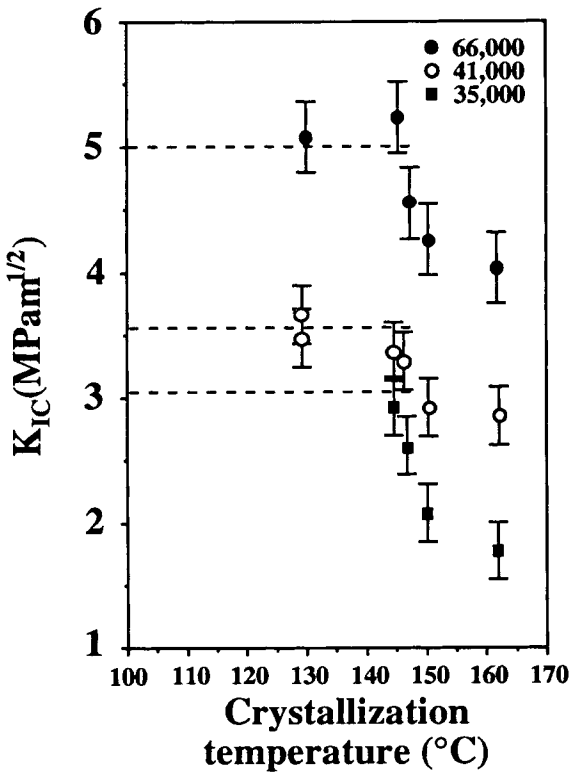

Figure 9 Experimental K_{IC} behavior at different crystallization temperatures.

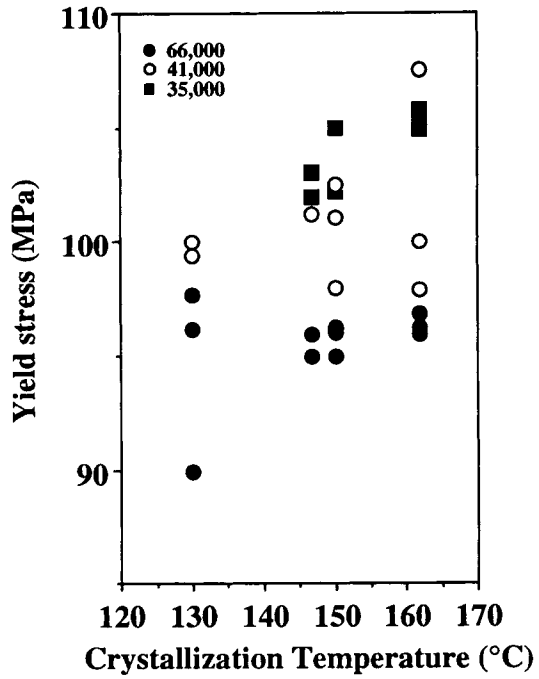

Figure 10 Experimental compressional yield stress at different crystallization temperatures.

in acceptable agreement with that obtained from samples crystallized in the DSC, the higher molecular weight plaques showed multiple melting peaks, with an upper melting point not exceeding 175°C. It must therefore be inferred that these latter had only undergone partial crystallization at 160°C. T_c for the injection-molded plaques was estimated from heat-transfer calculations to be approximately 130°C (Ref. 20) (note that for injection moldings and for crystallization temperatures lower than 150°C, the DSC melting point is always about 172°C owing to recrystallization).

The results of the mechanical tests shown in Figures 9 and 10, where initiation values of K_{IC} (subsequent crack propagation was unstable in all cases) and the compression yield stress are given for the different molecular weights and estimated T_c. The K_{IC} data points for T_c = 147, 150, and 160°C and the injection moldings represent averages for four samples, whereas those for 140°C were for four different plaques. The error bars indicate the range of scatter of the individual data points, and all the results conformed with the criteria set out in Ref. 9 for valid K_{IC} measurement (the departure from linearity of the force-displacement curves was generally well below 5%). The yield stress showed relatively little increase with the estimated values of T_c and with decreasing molecular weight. K_{IC}, on the other

hand, dropped sharply with increasing T_c and decreasing molecular weight. There was no evidence that crack paths followed the spherulite boundaries, and the deformation zones visible at the tips of the precracks were uniform in length.

Estimates of the plastic zone size using $r_p = (1/6\pi)(K_{IC}/\sigma_y)^2$ and the length of the deformation zones estimated from SEM observation of the fracture surfaces are compared in Table II, where these latter could be clearly identified. In the compression-molded samples, the plastic zone size was consistently less than the spherulite size (between 160 and 200 μm). The injection-molded samples, on the other hand, had somewhat finer microstructures. Although this is clearly symptomatic of the faster cooling rates, there is no a priori reason to attribute the higher K_{IC} of the injection moldings to this change in microstructure. This is consistent with the conclusions of other authors, who have linked variations in fatigue resistance in POM with variations in tie molecule density rather than changes in the coarse microstructure.[33]

The similarity between the measured and predicted dependence of K_{IC} on T_c in Figures 8 and 9 is encouraging, in spite of the considerable uncertainty surrounding the crystallization conditions. The prediction of the molecular weight dependence is less good. It is true that the calculations on which Figure 8 is based assume monodispersity and make use of M_n rather than M_w, for which no data were available, although we believe the grades to have a polydispersity of approximately 2. Recent calculations have, in fact, suggested that this will lead to relatively small changes in $K_{IC}(T_c)$[35] and it does not appear to account for the molecular weight dependence of K_{IC} at fixed T_c.

Given the relative insensitivity of the room-temperature yield stress to strain rate,[3] disentanglement would not be expected to play an important role in any entanglement loss during the formation of the fibrils (this would also be consistent with observations of stable macroscopic necks in rapidly cooled PE, whose extension ratios at room temperature correspond approximately to those predicted from the melt entanglement density[36]). There does exist the possibility of entanglement loss by chain scission during voiding at the crack tip, as in crazing in amorphous polymers,[4,5] but if, as suggested in Refs. 1–3, void spacings are of the order of 0.1 μm, i.e., much greater than d_e, molecular weight degradation and entanglement loss is not expected to be severe.

Table II Calculated and Measured Plastic Zone Sizes in μm for Different T_c and M_n

	r_p Calcd			r_p Measured		
T_c	66,000	41,000	35,000	66,000	41,000	35,000
130	161	78	—	200	100	—
147	122	55	34	—	—	—
150	106	43	21	85	50	25
160	94	40	15	53	—	—

This does not, however, rule out the possibility that subsequent fibril breakdown occurs by disentanglement, so that we have a molecular weight dependent f_s. Although the phenomenology of deformation in POM is not immediately suggestive of crack tip advance by disentanglement (K_{IC} is relatively temperature-insensitive to T at room temperature and below, and drops with increasing strain rate[8]), it would account for the relatively strong M dependence of K_{IC}. In models for craze breakdown by disentanglement in amorphous polymers, e.g., an $M^{3/2}$ dependence is predicted for the mean force in the chain, when it first starts to disentangle (corresponding to the maximum force that can be supported by the fibril[5,37,38]). In the present case, the frictional forces that oppose large-scale chain slip are likely to arise from the presence of the lamellae, rather than viscous forces in the amorphous regions (which are well above their T_g). However, as in the amorphous case, it is reasonable to assume the ultimate strength of a fibril to be given by the mean force in the moving chains multiplied by the surface density of load-bearing strands in the amorphous regions.

Given that the degree of crystallinity in the fibrils is likely to decrease with molecular weight, the M dependence of disentanglement forces may be weaker than in the amorphous case. Indeed, comparison of Figures 9 and 8 suggests that f_s would have to scale as approximately $M^{1/2}$ to account for the experimental results in terms of the model. One should, of course, be wary of too detailed an interpretation of this, both in view of the approximations and assumptions involved and also given that the samples are polydisperse and that the available range of molecular weights is limited for POM.

CONCLUSION

We have based our estimates of the crystallization temperature dependence of K_{IC} for crack initiation in POM on the assumption of nucleation-controlled growth in the range of crystallization temperatures constituting our processing window and on a fracture

criterion based on entanglement density. Hoffman's interpretation of spherulite growth rates in POM as a function of T_c (Ref. 21) was cited in support of the first assumption. Given the controversy currently surrounding kinetic theories of crystallization, the question of the extent to which this is really justified is a thorny one, although as discussed in the section Predicting Entanglement Loss During Crystallization nonacceptance of Hoffman's theory need not invalidate the qualitative conclusions. We have therefore tried to distance ourselves as much as possible from specific reference to such theories in the subsequent analysis.

It was argued that where spherulite or lamellar growth is controlled by secondary nucleation, a form of forced reptation may still occur in the earlier stages of crystallization of a given chain. This further implies entanglement loss, an effect that we have estimated by assuming the chains to continue to be reeled out of their tubes until the number of nucleation events along a given chain results in effective pinning of the chain. At relatively low crystallization temperatures, spherulite growth is considered to be too rapid to allow even transient reptation, and so it is assumed that the entanglement network is unperturbed by crystallization (entanglements may be rejected into the amorphous layers between lamellae, but only by "reeling-in of slack"; hence, the overall number of entanglements remains approximately constant). The injection moldings are argued to correspond to this condition.

Compression moldings crystallized at higher temperatures show diminished K_{IC} values that are argued to result from disentanglement during lamellar folding, leading, in turn, to a decrease in the number of load-bearing molecular bridges in the amorphous layers. The observed molecular weight dependence of K_{IC} may arise, in part, from the chain end correction to the effective entanglement density and to the molecular weight dependence of disentanglement during crystallization. However, the discrepancy between the predicted and observed molecular weight dependence suggests that chain slip may be mediating fibril breakdown in POM. Assuming little entanglement loss or chain slip during fibril formation, the ultimate strength of the fibrils is thus the mean force necessary to activate chain slip (presumed molecular weight-dependent) multiplied by the effective surface density of entangled strands.

On the basis of our approach, the properties of rapidly cooled injection moldings represent the optimum as far as the fracture toughness of pure POM under SSY conditions is concerned, with some improvement to be expected on increasing the molecular weight, at the expense of a slight decrease in tensile strength and modulus owing to the lower crystallinity. There no direct link between spherulite size, and toughness is implied. Although fine microstructures are generally symptomatic of high cooling rates and are, hence, likely to be associated with improved toughness, the present model does not provide a basis for the use of nucleation agents to improve resistance to crack initiation in POM.

Among factors worthy of more attention are molecular weight segregation during crystallization, the possibility of disentanglement during lamellar thickening, and molecular weight degradation during processing. It would, e.g., be interesting to compare isothermally crystallized and annealed samples having the same lamellar thickness. At a practical level, better control is needed of the crystallization temperature, which would inevitably mean turning to a film geometry, since this is essentially a heat-transfer problem. The essential work method appears promising in this respect, although it remains to be seen to what extent the mechanisms of fracture in such a geometry will reflect those of the bulk.

We acknowledge the financial support of the Swiss Council for the Encouragement of Research and DuPont de Nemours Ltd. and Dr. C. Creton for valuable discussions.

REFERENCES

1. I. Narisawa and M. Ishikawa, in *Advances in Polymer Science,* H.-H. Kausch, Ed., Springer-Verlag, Berlin, 1990, Vols. 91/92, Chap. 8.
2. E. A. Flexman, in *Toughened Plastics: Science and Engineering,* ACS Advances in Chemistry Series, C. K. Riew and A. J. Kinloch, Eds., American Chemical Society, Washington, DC, 1993, p. 79.
3. C. J. G. Plummer, N. Cudré-Mauroux, and H.-H. Kausch, *J. Polym. Sci. Eng.,* **34,** 318 (1994).
4. E. J. Kramer, in *Advances in Polymer Science,* H.-H. Kausch, Ed., Springer-Verlag, Berlin, 1983, Vols. 52/53, Chap. 1.
5. E. J. Kramer and L. L. Berger, in *Advances in Polymer Science,* H.-H. Kausch, Ed., Springer-Verlag, Berlin, 1990, Vols. 91/92, Chap. 1.
6. H. R. Brown, *Macromolecules,* **24,** 2752 (1991).
7. C. Y. Hui, A. Ruina, C. Creton, and E. J. Kramer, *Macromolecules,* **25,** 3948 (1992).
8. C. J. G. Plummer, P. Béguelin, and H.-H. Kausch, *Proceedings of the European Symposium on Impact and Dynamic Fracture of Polymers and Composites,* Porto Cervo, Italy, September, 1993, to appear.
9. "A Linear Elastic Fracture Mechanics Standard for Determining K_c and G_c for Plastics," European Structural Integrity Society, 1992.

10. J. G. Williams, *Trans. J. Plast. Inst.*, **June,** 505 (1967).
11. A. Franbourg and F. Reitsch, *Makromol. Chem.*, **91,** 269 (1990).
12. F. Rybnikar, *Collect. Czech. Chem. Commun.*, **31,** 4080 (1966).
13. Z. Pelzbauer and A. Galeski, *J. Polym. Sci. C,* **38,** 23 (1972).
14. T. Amano, E. W. Fischer, and G. Hinrichsen, *J. Macromol. Sci.-Phys.*, **B3**(2), 209 (1969).
15. F. Salaris, A. Turturro, U. Bianchi, and E. Martuscelli, *Polymer,* **19,** 1163 (1978).
16. J. Brandrup and E. H. Immergut, Eds., *Polymer Handbook,* Wiley, New York, 1989.
17. A. Keller, in *Proceedings of the 17th Europhysics Conference on Macromolecular Physics,* July 1985, B. Sedláček, Ed., Walter de Gruyter, Berlin, 1988, Vol. 2.
18. J. I. Lauritzen and J. D. Hoffman, *J. Res. Nat. Bur. Std.*, **64A,** 73 (1960).
19. D. C. Bassett, *Principles of Polymer Morphology,* Cambridge University Press, Cambridge, 1981.
20. C. L. Soles and C. J. G. Plummer, unpublished results, 1994.
21. J. D. Hoffman, *Polymer,* **24,** 3 (1983).
22. J. D. Hoffman and R. L. Miller, *Macromolecules,* **21,** 3038 (1988).
23. P. J. Flory and D. Y. Yoon, *Nature,* **272,** 16 (1978).
24. J. Schelten, D. G. H. Ballard, G. D. Wignall, G. Longman, and W. Schmatz, *Polymer,* **17,** 751 (1976).
25. J.-M. Guenet, *Polymer,* **22,** 313 (1981).
26. J. J. Point and M. Dosière, *Polymer,* **30,** 2292 (1989).
27. D. M. Sadler, *Polymer,* **28,** 1440 (1987).
28. J. J. Point and D. Villers, *Polymer,* **33,** 2263 (1992).
29. J. Klein and R. Ball, *Faraday Soc. Discuss.*, **68,** 198 (1979).
30. P. G. DeGennes, *J. Chem. Phys.*, **55,** 572 (1971).
31. D. W. Van Krevelen, *Properties of Polymers,* Elsevier, Amsterdam, 1976.
32. C. M. Guttman, E. A. Dimarzio, and J. D. Hoffman, *Polymer,* **22,** 1466 (1981).
33. J. Runt and K. P. Gallagher, *J. Mater. Sci.*, **26,** 792 (1991).
34. U. W. Gedde and J. F. Jansson, *Polymer,* **26,** 1471 (1985).
35. C. J. G. Plummer and H.-H. Kausch, presented at the seminar "Self Organization in Polymers," The Royal Society, December 1994, London, U.K. Royal Society, 1994.
36. Y. Termonia, S. R. Allen, and P. Smith, *Macromolecules,* **21,** 3485 (1988).
37. C. J. G. Plummer and A. M. Donald, *Polymer,* **32,** 409 (1991).
38. T. C. B. McLeish, C. J. G. Plummer, and A. M. Donald, *Polymer,* **30,** 1651 (1989).

Received November 11, 1993
Accepted August 1, 1994